

Research Article

Selective Synthesis and Luminescence Properties of Nanocrystalline $\text{GdF}_3:\text{Eu}^{3+}$ with Hexagonal and Orthorhombic Structures

Xiaoting Zhang,¹ Tomokatsu Hayakawa,¹ Masayuki Nogami,¹ and Yukari Ishikawa^{1,2}

¹ Field of Advanced Energy Conversion, Department of Frontier Materials, Nagoya Institute of Technology, Gokiso, Showa-ku, Nagoya 466-8555, Japan

² Japan Fine Ceramics Center, 2-4-1 Mutsuno, Atsuta-ku, Nagoya 456-8587, Japan

Correspondence should be addressed to Tomokatsu Hayakawa, hayatomo@nitech.ac.jp

Received 3 August 2010; Accepted 16 October 2010

Academic Editor: Rakesh Joshi

Copyright © 2010 Xiaoting Zhang et al. This is an open access article distributed under the Creative Commons Attribution License, which permits unrestricted use, distribution, and reproduction in any medium, provided the original work is properly cited.

$\text{GdF}_3:\text{Eu}^{3+}$ nanophosphors with hexagonal or orthorhombic structure have been succeeded to be selectively synthesized at room temperature for the first time via a simple soft chemical route. The structure and morphology of $\text{GdF}_3:\text{Eu}^{3+}$ nanophosphors were controlled by using different fluoride precursors. Hexagonal $\text{GdF}_3:\text{Eu}^{3+}$ nanocrystals were formed when NaBF_4 was used as a fluoride precursor, while orthorhombic $\text{GdF}_3:\text{Eu}^{3+}$ nanocrystals were obtained with NaF or NH_4F fluoride precursor. It was also experimentally revealed that hexagonal $\text{GdF}_3:\text{Eu}^{3+}$ nanophosphors emitted essentially stronger Eu^{3+} luminescence than orthorhombic ones did. The formation mechanism of GdF_3 nanocrystals and the possible reasons of the strong PL in hexagonal were discussed.

1. Introduction

In recent years, precise architectural manipulation of lanthanide trifluorides (LnF_3) nanocrystals gathers great attention because nanostructure-based properties were closely interrelated with geometrical factors such as crystal structure, shape, dimensionality, and size [1–6]. Various techniques recently used to control shape and size of lanthanide trifluorides nanoparticles were also summarized by Rahman and Green [3]. Above all, polytype control of LnF_3 becomes one of the most interesting issues to improve light emitting properties as intra f - f transitions of lanthanide ion are affected by the coordination of atoms around the lanthanide atom. Mansmann [7] pointed out that the polytypes of LnF_3 (hexagonal or orthorhombic) depend on ionic radius and coordination number of the lanthanide metal. An increase in a repulsive energy between fluoride ions with a decrease in an ionic radius of lanthanide (r_{Ln}) results in polytype change from hexagonal to orthorhombic. A critical ratio of $r_{\text{Ln}}/r_{\text{F}}$ was proposed to be 0.94. Taking into account the

ionic radius calculated by Ahrens [8], the critical point is positioned between Sm and Eu. However, it was reported that the critical point of LnF_3 polytype in an aluminosilicate was experimentally between Gd and Tb [9], which is supported on the basis of the Shannon's table for ionic radii [10]. Resultantly, it can be known that polytype control of GdF_3 is fundamentally possible and GdF_3 is a proper material for investigating the influence of polytype on the light emitting properties of lanthanide activator doped such as Eu^{3+} , Tb^{3+} , and Sm^{3+} . Because of its potential in optical and biological application, GdF_3 has attracted much increasing attention as a good host lattice [4–6, 9], and actually polytype GdF_3 crystals had been prepared [11–13]. However, they were synthesized at high temperature, and how the polytype structure influences luminescence properties is still unknown.

We report here, for the first time to our best knowledge, that polytype GdF_3 nanocrystals can selectively be prepared at room temperature (RT) through a simple method. We will demonstrate the selective synthesis of hexagonal and

orthorhombic $\text{GdF}_3:\text{Eu}^{3+}$ by choosing fluoride precursors in controlled precipitation method at RT. Luminescence properties of nanostructured $\text{GdF}_3:\text{Eu}^{3+}$ are also reported. These nanophosphors are characterized by X-ray diffraction (XRD), Scanning Electron Microscopy (SEM), Transmission Electron Microscopy (TEM), Energy Dispersive X-ray spectroscopy (EDX), and Photoluminescence (PL) measurements.

2. Experimental

All reagents were obtained from Aldrich Chem. CO. and were used as starting materials without further purification. Typical procedure for the synthesis of $\text{GdF}_3:\text{Eu}^{3+}$ nanocrystals is described as follows. First, 0.005 mol $\text{Gd}(\text{NO}_3)_3 \cdot 6\text{H}_2\text{O}$ and 0.0025 mol $\text{EuCl}_3 \cdot 6\text{H}_2\text{O}$ were dissolved in 100 mL deionized water in a beaker at RT. After being stirred mechanically for about 20 min, 0.015 mol NaBF_4 (sample A), 0.015 mol NaF (for sample B), and 0.015 mol NH_4F (for sample C) aqueous solutions were added dropwise, respectively, under constant stirring for 12 h at RT. The final product was collected by centrifugation and washed subsequently with water and ethanol three times, respectively. After the centrifugation the particles were dried in an oven at 80°C . Nominal Eu^{3+} concentration was 5 mol%.

X-ray diffraction (XRD) measurements were performed on a Phillips X'pert system using $\text{CuK}\alpha$ radiation with 45 kV voltage and 40 mA current. The morphology, size, and Eu^{3+} concentration of the products were examined by a scanning electron microscopy of HITACHI S-4500 microscope equipped with EDX (EMAX-7000). The structural characteristics of the samples were further examined with a transmission electron microscope (JEOL, JEM-4000FX) using an accelerating voltage of 400 kV. The excitation and photoluminescence spectra were obtained by F-7000 fluorescence spectrophotometer (Hitachi, CO.).

3. Results and Discussion

Figure 1 shows the XRD profiles of the prepared $\text{GdF}_3:\text{Eu}^{3+}$ nanophosphors. In this figure, the XRD patterns of the sample A, B, and C are indicated as (a), (b), and (c), respectively. The XRD patterns of sample B is similar to that of sample C; these two patterns can be readily identified orthorhombic GdF_3 (PDF No.12-0788). It can be found that a (020) peak of sample B is sharper than that of sample C so that sample B seems to have better crystallinity. On the other hand, the XRD pattern of sample A clearly differs from those of B and C. Since the XRD data for the hexagonal GdF_3 have not been reported, this phase is compared with hexagonal SmF_3 (PDF No. 05-0563) and all the diffraction peaks in Figure 1(a) can be indexed to the hexagonal structure. The lattice constants, which can be determined by using the Bragg equation $d_{hkl} = n\lambda/2 \sin \theta$, are listed in Table 1.

Figure 2 shows SEM, TEM images, and Selected Area Electron Diffraction (SAED) pattern of sample A. SEM image in Figure 2(a) shows that the particles have “disc”-like morphology [14] with size about 0.9–1.5 μm in diameter. A

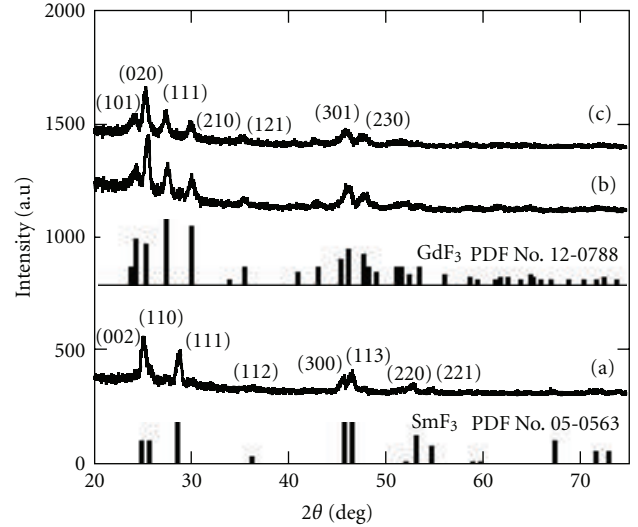


FIGURE 1: XRD patterns of the samples synthesized with (a) NaBF_4 , (b) NaF , and (c) NH_4F .

TABLE 1: Lattice constants of $\text{GdF}_3:\text{Eu}^{3+}$ nanocrystals, obtained from XRD data.

Sample	Structure	Lattice constant		
		a/nm	b/nm	c/nm
A	Hexagonal	0.6998	0.6998 (=a)	0.6813
B	Orthorhombic	0.6557	0.6967	0.4388
C	Orthorhombic	0.6571	0.6985	0.4393

TEM image in Figure 2(b) elucidates the unique morphology the same as the SEM image. From the magnified TEM image in the inset of Figure 2(b), it can be seen that this round shape is brought by aggregate of “plate”-like clusters. The SAED patterns in Figure 2(c) indicate that there are two kinds of clusters in a disc-like particles, which have the same SAED pattern in hexagonal. The lattice constant of one kind of clusters was $a = b = 0.5926 \text{ nm}$, and that of the other kind of clusters was $a = b = 0.6928 \text{ nm}$. It should be noted that both clusters belonged to a hexagonal crystal system in spite of the difference of lattice constant and each other kept epitaxial relationship. Images of SEM and TEM of sample B and C are obtained and shown in Figure 3. For sample B, SEM image (Figure 3(a)) and TEM image (Figure 3(b)) show that the particles exhibited a round shape with a hole in it and the particle size was about 0.8–1.2 μm in diameter, estimated from the magnified TEM image (see the inset of Figure 3(b)). It can be clearly seen that this round shape is formed due to clustered “hair”-like nanoparticles. The SEM image (Figure 3(c)) and TEM image (Figure 3(d)) of sample C shows “spindle”-like morphology with dimensions of 300–400 nm in length and 60–100 nm in width. SAED pattern of sample C is shown in Figure 4, which indicates that spindle-like clusters were orthorhombic and almost aligned like a single crystal, but it contained slightly tilted ones toward (011). The lattice constants of b and c were 0.6978 nm

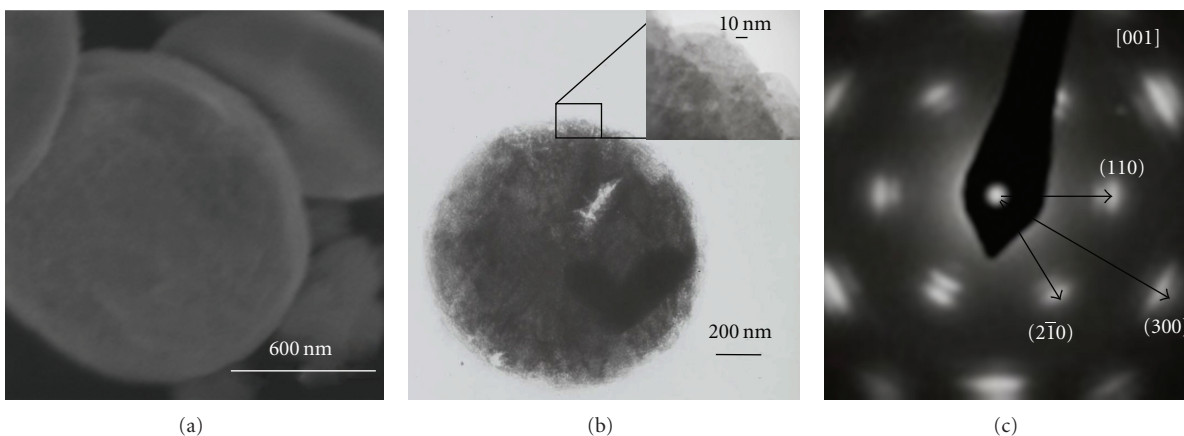


FIGURE 2: SEM image (a), TEM image (b) and SAED pattern (c) of sample A (Inset shows the magnified TEM image (b)).

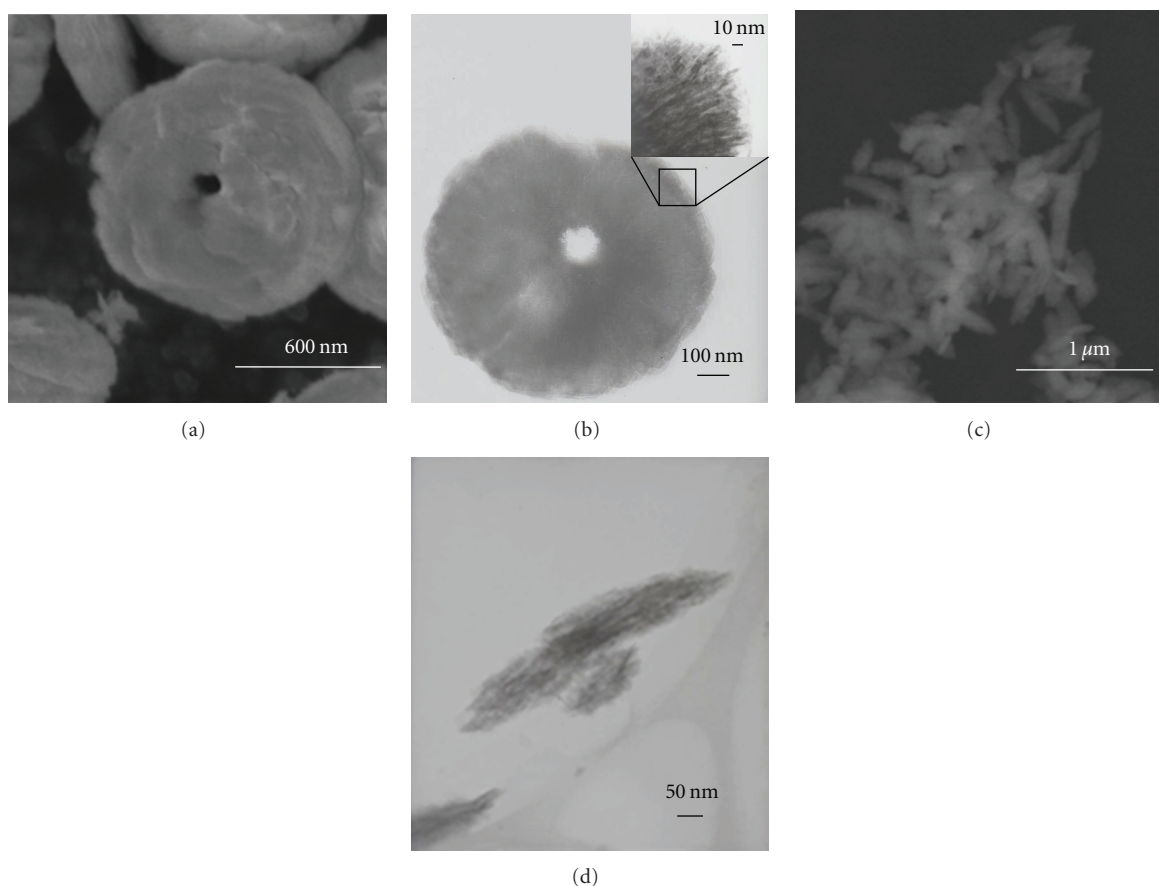


FIGURE 3: SEM image (a) and TEM image (b), (inset shows the magnified TEM image) of sample B, SEM image (c), and TEM image (d) of sample C.

and 0.4433 nm, respectively, which is consistent with the estimation given from XRD (see Table 1).

As shown above, the crystal structures and morphologies of $\text{GdF}_3\cdot\text{Eu}^{3+}$ nanoparticles depended on the fluoride source, even though the synthetic conditions were identical except for the fluoride sources. Recent investigations also demonstrated the formation of hexagonal and orthorhombic GdF_3 nanocrystals; however, these nanocrystals were synthesized

at higher temperatures ($>300^\circ\text{C}$) [11–13, 15]. Our method is very simple and employed at room temperature, where it is demonstrated that different fluoride sources have the strong impacts not only on morphologies but also on crystal structures of GdF_3 nanocrystals.

Here, we emphasized the crucial effect of NaBF_4 on the crystalline phases of the products in our current synthesis. In the case of NaF and NH_4F , a white precipitate appeared

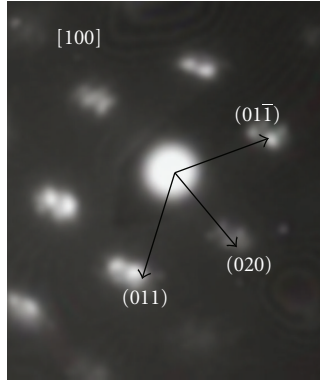
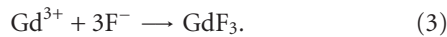
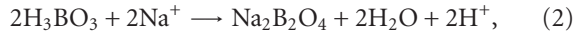
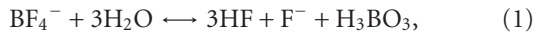


FIGURE 4: SAED pattern of sample C.

immediately after the gadolinium nitrate solution was mixed with sodium or ammonium fluoride, which indicated that the nucleation had taken place rapidly. On the other hand, the initial solution was kept clear and transparent when NaBF_4 was added as a fluoride source, suggesting that no fluoride precipitation was formed. The white precipitate was formed after stirring for 20 min. The probable reaction processes for the formation of GdF_3 can be summarized as follows:



In an aqueous solution, NaBF_4 was slowly hydrolyzed to produce BO_3^{3-} and F^- anions, as shown in (1), as the equilibrium constant of the hydrolysis reaction was very small ($K_\theta = 6.41 \times 10^{-12}$ at 25°C) [16] and the concentration of F^- anions in the reaction solution was kept at a low level [17, 18], from the view of the reaction equilibrium, and so the low F^- concentration is brought in an acidic environment. Furthermore, the composition analysis of the clear solution after centrifugation demonstrated the formation of H_3BO_3 and $\text{Na}_2\text{B}_2\text{O}_4$ (2). The pH value of the aqueous solution was approximately equal to 6.0 at the beginning of the reaction, and when the reaction was complete the pH value decreased to 1.5. Finally, Gd^{3+} ions were reacted with F^- anions produced during the slow hydrolysis of NaBF_4 , so as to form GdF_3 nuclei, as presented in (3). Because of the very low production rate of F^- anions in solution, the particle growth of the precipitated GdF_3 solid was very slow. Additionally, the hexagonal-structure could be stabilized if the fluorine anions were deficient [7], so the deficiency of F^- anions due to the low F^- concentration in solution might help synthesize hexagonal structure.

Room temperature PL spectra are presented in Figure 5 and the luminescence bands are assigned according to Carnall's paper [19]. Emission spectra has shown two intense bands associated with $^5\text{D}_0 \rightarrow ^7\text{F}_1$ and $^5\text{D}_0 \rightarrow ^7\text{F}_2$ transitions for Eu^{3+} . The peak centered at 592 nm corresponds

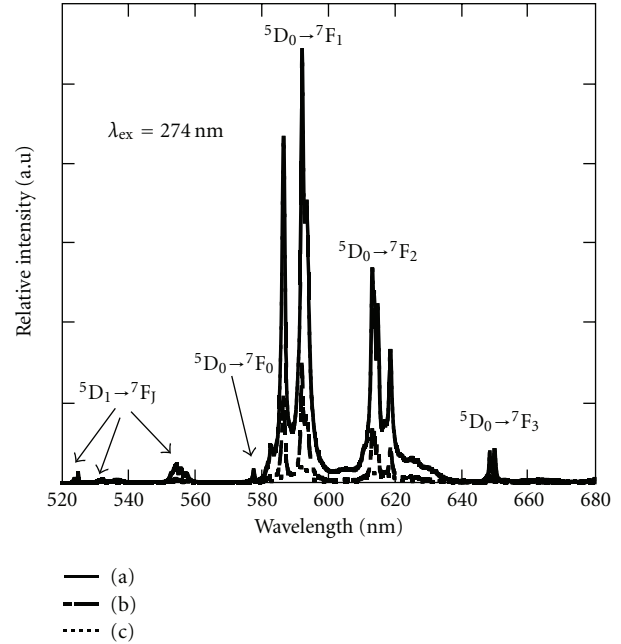


FIGURE 5: Photoluminescence spectra of $\text{GdF}_3:\text{Eu}^{3+}$ nanocrystals for different samples ((a) hexagonal, (b), and (c) orthorhombic).

to the $^5\text{D}_0 \rightarrow ^7\text{F}_1$ magnetic dipole transition, and the peak centered at 619 nm corresponds to the $^5\text{D}_0 \rightarrow ^7\text{F}_2$ electric dipole transition. The little peaks located at 525 nm, 530 nm, and 554 nm were corresponding to the $^5\text{D}_1 \rightarrow ^7\text{F}_1$ transitions [20]. Interestingly, the intensity of the 592 nm PL from hexagonal sample A was much larger than that of orthorhombic samples of B and C.

EDX spectra of the samples studied were shown in Figure 6. Peaks located at about 5.845 keV and 6.056 keV were assigned to the $\text{Eu L}_{\alpha 1}$ and $\text{Gd L}_{\alpha 1}$, respectively. The spectra indicated that Eu concentrations in $\text{GdF}_3:\text{Eu}^{3+}$ were independent on the fluoride sources and a bit decreased from the nominal value (5 mol%) to 4.2–4.4 mol%. In was found that the obtained $\text{GdF}_3:\text{Eu}^{3+}$ nanophosphors had the almost same Eu^{3+} concentration. Therefore, it can be concluded that the stronger PL intensity of hexagonal sample A than these of orthorhombic sample B and C would be caused by the polytype host GdF_3 . In order to examine the compounds purity, we have detected EDX and Fourier Transform-Infrared (FT-IR) spectra. In EDX spectra (not shown here), no peaks from Na and N elements can be found so that Na and N elements concentrations in particles are too low to be detected. Thus, NaGdF_4 and NH_4GdF_4 have not been produced during the synthesis, and even if they exist, they are so little and can be ignored. It can also be found that hexagonal GdF_3 nanocrystals have higher O-to-Gd (O/Gd) elemental ratio (4.18) than orthorhombic GdF_3 nanocrystals does (1.47 in sample B and 1.23 in sample C). It is because the samples were prepared in aqua solution and without postannealing treatment, and so OH^- ions and/or H_2O absorbed on the crystals surface could not be removed completely. Some OH^- ions and/or H_2O

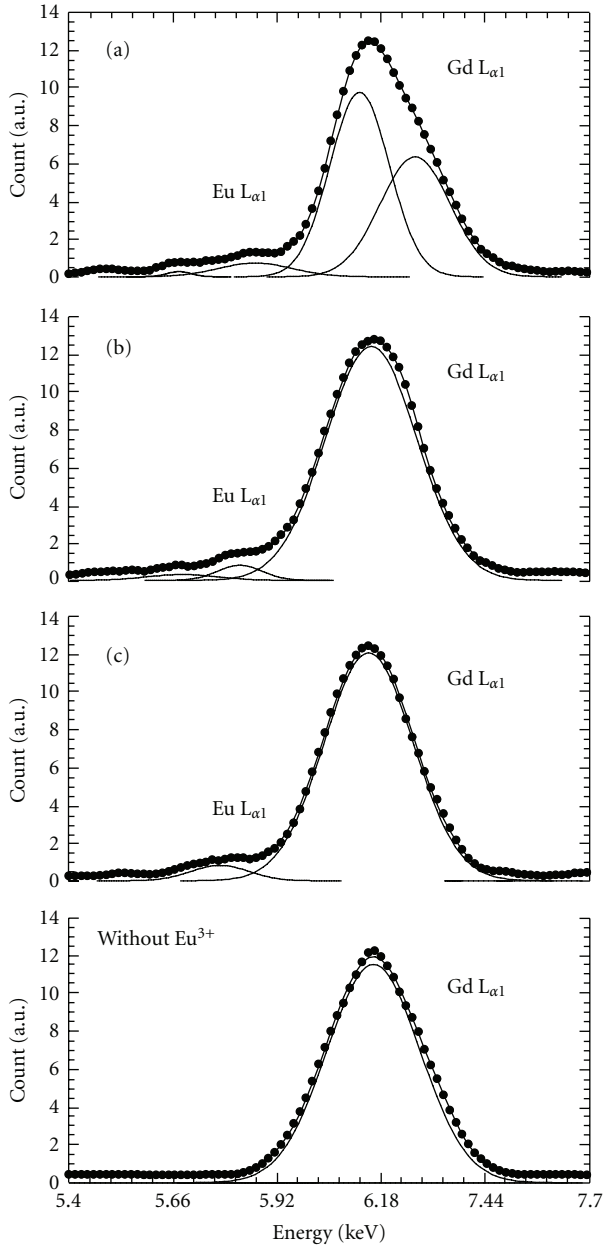


FIGURE 6: EDX spectra of different samples (a), (b), (c) and without Eu^{3+} .

molecules were more or less residual in the samples. As for the high O-to-Gd ratios over 1, it can be commented out that since EDX elemental analysis takes data from crystals surface, and OH^- and/or H_2O absorbed on crystals surface were predominantly detected. As a result, it is found that O concentration is higher in hexagonal crystals than in orthorhombic crystals. The same results can also be obtained in FT-IR spectra (not shown here), where the peak located at about 3150 cm^{-1} is associated to OH-stretching vibration, and the FT-IR intensity is stronger in hexagonal crystals than in orthorhombic crystals. From the result, it can be speculated that hexagonal GdF_3 nanocrystals might be stabilized by OH impurities. Moreover, it is important

to be emphasized here that although hexagonal $\text{GdF}_3:\text{Eu}^{3+}$ nanocrystals had relatively more impurities related with OH groups, they exhibited stronger luminescence intensity than orthorhombic $\text{GdF}_3:\text{Eu}^{3+}$ nanocrystals.

As it is known, in the structure of orthorhombic symmetry with space group $Pnma$ (No. 62), the Gd^{3+} ion lies in the center of an irregular trigonal prism with six fluoride ions at the corners. The three other fluoride ions are symmetrically disposed in front of the prism (as in Figure 7); therefore, the number of fluoride ions around Gd^{3+} ions is 9. On the other hand, in the hexagonal crystal structure ($P6_3/mcm$ (No.193)), there are more 2 other fluoride ions disposed up and down the prism, and thus the number of fluoride ions around Gd^{3+} becomes 11. An increase in the fluoride number contributes to the enhancement of ionic bonding character between the Gd^{3+} ions and the F^- ions. With reference to the previous work of Rotereau et al. [21], Raman spectrum peaks were shifted to the lower frequency when SmF_3 crystal structure was changed from orthorhombic to hexagonal structure; the highest-frequency vibration was decreased in energy (490 cm^{-1} (orthorhombic), 390 cm^{-1} (hexagonal)), and the phonon energy thus became lower. According to the energy-difference law equation, $W_{\text{nr}} = \beta e^{-\alpha(\Delta E - 2h\omega)}$, α and β are materials-dependent constants, ΔE is the energy difference associated with emission, and $h\omega$ is the maximum phonon energy [22, 23]. So, it is presumably concluded that the sample with a hexagonal crystal structure has a low nonradiative transition probability W_{nr} in comparison with orthorhombic $\text{GdF}_3:\text{Eu}^{3+}$ and finally results in the stronger luminescence. Further study is now in progress.

Figure 8 shows the excitation spectra of the $^5\text{D}_0 \rightarrow ^7\text{F}_2$ emission of Eu^{3+} in $\text{GdF}_3:\text{Eu}^{3+}$ (619 nm) at room temperature. The excitation spectra of the $^5\text{D}_0$ red emission indicate that the sharp peak located at 274 nm corresponds to excitation into $^6\text{I}_7$ ($J' = 7/2-17/2$) ($^8\text{S}_{7/2} \rightarrow ^6\text{I}_7$) levels of Gd^{3+} , and the peak located at 396 nm corresponds to the $^7\text{F}_0 \rightarrow ^5\text{L}_6$ direct excitation of Eu^{3+} . The short wavelength excitation confirms the occurrence of energy transfers from $^6\text{I}_7$ ($J' = 7/2-17/2$) level of Gd^{3+} to Eu^{3+} . The $4f$ energy level overlap between the $^6\text{P}_j$ states of Gd^{3+} and the $^5\text{H}_j$ states of Eu^{3+} allows energy transfer from Gd^{3+} to Eu^{3+} , and thus energy transfer route from Gd^{3+} to Eu^{3+} can be explained [5, 6, 12–15, 17, 18] as follows: Gd^{3+} ions are first excited to $^6\text{I}_7$ ($J' = 7/2-17/2$) energy level and through nonradiative relaxation decay to $^6\text{P}_j$ states, and then from this level transfer its excitation energy to Eu^{3+} ion, resulting in the emission of visible photons due to the Eu^{3+} : $^5\text{D}_0 - ^7\text{F}_j$ transition. Further study is now in progress. A detailed Reitveld refinement of X-ray diffraction patterns has been carried out to obtain more information on the phase purity, unit cell constants and strains. Very deep ultraviolet excitation of hexagonal and orthorhombic $\text{GdF}_3:\text{Eu}^{3+}$ nanocrystals is also planned and will be reported elsewhere.

4. Conclusions

In this paper, we proved that $\text{GdF}_3:\text{Eu}^{3+}$ nanocrystals with hexagonal and orthorhombic structure could separately be

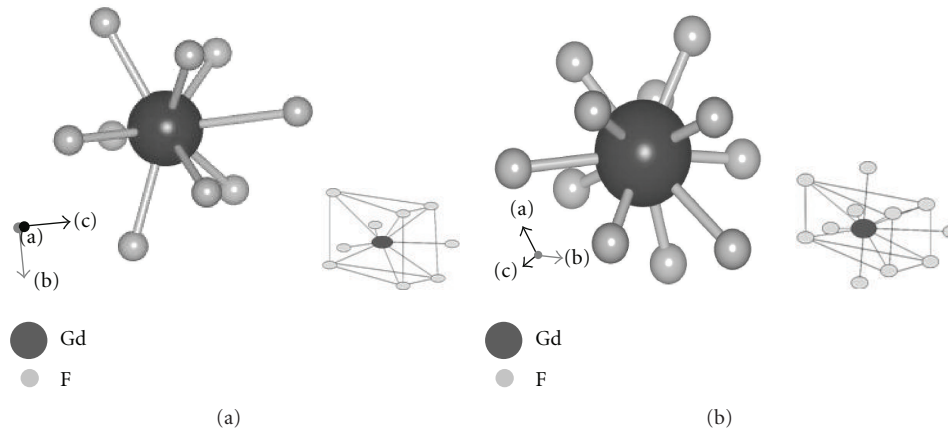


FIGURE 7: Orthorhombic crystal structure (a) and hexagonal crystal structure (b). The fractional coordinates used were given in [14].

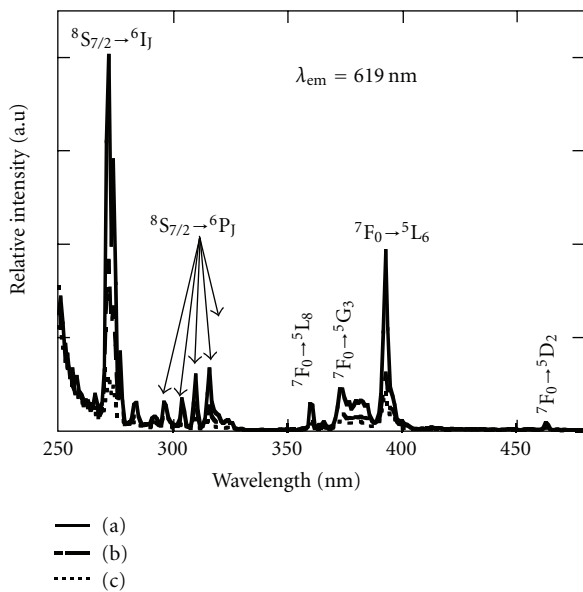


FIGURE 8: Photoluminescence excitation spectra of the $\text{GdF}_3:\text{Eu}^{3+}$ nanocrystals ((a) hexagonal, (b) and (c) orthorhombic).

synthesized at room temperature by using different fluoride precursors in precipitation method at room temperature. Hexagonal $\text{GdF}_3:\text{Eu}^{3+}$ nanocrystals were formed in “plate”-like morphologies when NaBF_4 was used as a fluoride precursor, while orthorhombic $\text{GdF}_3:\text{Eu}^{3+}$ nanocrystals in “hair”- and “spindle”-like morphologies were obtained with NaF or NH_4F fluoride precursor, respectively. We discussed on the formation mechanism of hexagonal $\text{GdF}_3:\text{Eu}^{3+}$ nanocrystals and explained it by the slow hydrolysis of NaBF_4 , the deficiency of fluorine anions, and the incorporation of OH^- impurities. The $^5\text{D}_0$ photoluminescence of Eu^{3+} doped under ultraviolet light excitation was explained by energy transfer from Gd^{3+} to Eu^{3+} ions. By means of our structural and PL analysis, it was elucidated that hexagonal $\text{GdF}_3:\text{Eu}^{3+}$ nanophosphors emitted intense PL from Eu^{3+} in comparison with orthorhombic $\text{GdF}_3:\text{Eu}^{3+}$ ones.

Acknowledgments

X. T. Zhang greatly appreciates Dr. R. Huang, Dr. Y. Sasaki, A. Suzuki, and M. Yabuta of JFCC for their support of experiments and fruitful discussion. This work was in part supported by the JSPS International Training Program (ITP), “Young Scientist-Training Program for World Ceramics Networks”, and by grant from Institute of Ceramics Research and Education (ICRE) in Nagoya Institute of Technology.

References

- [1] A. P. Alivisatos, “Semiconductor clusters, nanocrystals, and quantum dots,” *Science*, vol. 271, no. 5251, pp. 933–937, 1996.
- [2] Y. Ding, S.-H. Yu, C. Liu, and Z.-A. Zang, “3D architectures of iron molybdate: phase selective synthesis, growth mechanism, and magnetic properties,” *Chemistry*, vol. 13, no. 3, pp. 746–753, 2007.
- [3] P. Rahman and M. Green, “The synthesis of rare earth fluoride based nanoparticles,” *Nanoscale*, vol. 1, no. 2, pp. 214–224, 2009.
- [4] X. Fan, D. Pi, F. Wang, J. Qiu, and M. Wang, “Hydrothermal synthesis and luminescence behavior of lanthanide-doped GdF_3 nanoparticles,” *IEEE Transactions on Nanotechnology*, vol. 5, no. 2, pp. 123–128, 2006.
- [5] T. Grzyb and S. Lis, “Photoluminescent properties of $\text{LaF}_3:\text{Eu}^{3+}$ and $\text{GdF}_3:\text{Eu}^{3+}$ nanoparticles prepared by coprecipitation method,” *Journal of Rare Earths*, vol. 27, no. 4, pp. 588–592, 2009.
- [6] M. M. Lezhnina, T. Jüstel, H. Kätker, D. U. Wiechert, and U. H. Kynast, “Efficient luminescence from rare-earth fluoride nanoparticles with optically functional shells,” *Advanced Functional Materials*, vol. 16, no. 7, pp. 935–942, 2006.
- [7] M. Mansmann, “Die kristallstruktur von lanthantrifluorid,” *Zeitschrift für Kristallographie*, vol. 122, pp. 375–398, 1965.
- [8] L. H. Ahrens, “The use of ionization potentials Part 1. Ionic radii of the elements,” *Geochimica et Cosmochimica Acta*, vol. 2, no. 3, pp. 155–169, 1952.
- [9] D. Chen, Y. Yu, P. Huang, and Y. Wang, “Nanocrystallization of lanthanide trifluoride in an aluminosilicate glass matrix: dimorphism and rare earth partition,” *CrystEngComm*, vol. 11, no. 8, pp. 1686–1690, 2009.

- [10] R. D. Shannon, "Revised effective ionic radii and systematic studies of interatomic distances in halides and chalcogenides," *Acta Crystallographica*, vol. 32, pp. 751–767, 1976.
- [11] S. V. Stankus, R. A. Khairulin, and K. M. Lyapunov, "Phase transitions and thermal properties of gadolinium trifluoride," *Journal of Alloys and Compounds*, vol. 290, no. 1-2, pp. 30–33, 1999.
- [12] D. Chen, Y. Wang, N. Yu, and P. Huang, "Structure and optical spectroscopy of Eu-doped glass ceramics containing GdF_3 nanocrystals," *Journal of Physical Chemistry C*, vol. 112, no. 48, pp. 18943–18947, 2008.
- [13] S. Fujihara, S. Koji, and T. Kimura, "Structure and optical properties of $(\text{Gd,Eu})\text{F}_3$ -nanocrystallized sol-gel silica films," *Journal of Materials Chemistry*, vol. 14, no. 8, pp. 1331–1335, 2004.
- [14] M. Wang, Q. L. Huang, J. M. Hong, X. T. Chen, and Z. L. Xue, "Selective synthesis and characterization of nanocrystalline EuF_3 with orthorhombic and hexagonal structures," *Crystal Growth and Design*, vol. 6, no. 8, pp. 1972–1974, 2006.
- [15] L. Zhu, Q. Li, X. Liu et al., "Morphological control and luminescent properties of CeF nanocrystals," *Journal of Physical Chemistry C*, vol. 111, no. 16, pp. 5898–5903, 2007.
- [16] Crooks W. J. III and W. D. Rhodes, Westinghouse Savannah River Company Aiken, SC 29808, WSRC-TR-2002–00462, 2003.
- [17] Z. J. Miao, Z. M. Liu, K. L. Ding, B. X. Han, S. D. Miao, and G. M. An, "Controlled fabrication of rare earth fluoride superstructures via a simple template-free route," *Nanotechnology*, vol. 18, pp. 125605–125609, 2007.
- [18] L. Zhu, J. Meng, and X. Cao, "Facile synthesis and photoluminescence of europium ion doped LaF nanodisks," *European Journal of Inorganic Chemistry*, no. 24, pp. 3863–3867, 2007.
- [19] W. T. Carnall, P. R. Fields, and K. Rajnak, "Electronic energy levels of the trivalent lanthanide aquo ions. IV. Eu," *The Journal of Chemical Physics*, vol. 49, no. 10, pp. 4424–4442, 1968.
- [20] X. T. Zhang, T. Hayakawa, and M. Nogami, "Photoluminescence properties and $^5\text{D}_0$ decay analysis of $\text{LaF}_3:\text{Eu}^{3+}$ nanocrystals prepared by using surfactant assist," *International Journal of Applied Ceramic Technology*. In press.
- [21] K. Rotereau, P. H. Daniel, A. Desert, and J. Y. Gesland, "The high-temperature phase transition in samarium fluoride, SmF : structural and vibrational investigation," *Journal of Physics Condensed Matter*, vol. 10, no. 6, pp. 1431–1446, 1998.
- [22] P. A. Rodnyi, "Cascade photon emission in luminophores," *Optics and Spectroscopy*, vol. 89, no. 4, pp. 556–562, 2000.
- [23] C. B. Layne, W. H. Lowdermilk, and M. J. Weber, "Multi-phonon relaxation of rare-earth ions in oxide glasses," *Physical Review B*, vol. 16, no. 1, pp. 10–20, 1977.



Hindawi

Submit your manuscripts at
<http://www.hindawi.com>

